

Short period variable stars in young open cluster Stock 8

SNEH LATA,¹ ANIL. K. PANDEY,¹ RAM KESH YADAV,² ANDREA RICHICHI,³ PUJI IRAWATI,² NEELAM PANWAR,¹
V. S. DHILLON,^{4,5} AND T. R. MARSH⁶

¹*Aryabhata Research Institute of Observational Sciences, Manora Peak, Nainital 263002, Uttarakhand, India*

²*National Astronomical Research Institute of Thailand, 191 Siriphanich Bldg., Huay Kaew Rd., Suthep, Muang, Chiang Mai 50200, Thailand*

³*INAF Osservatorio Astrofisico di Arcetri, Largo E. Fermi 5, I-50125 Firenze, Italy*

⁴*University of Dept of Physics & Astronomy, University of Sheffield, Sheffield S3 7RH, UK*

⁵*Instituto de Astrofísica de Canarias, E-38205 La Laguna, Tenerife, Spain*

⁶*Department of Physics, University of Warwick, Coventry CV4 7AL, UK*

(Received; Revised; Accepted)

Submitted to AAS

ABSTRACT

We present time series photometry in the field of Stock 8 and identified 130 short period variable stars. Twenty eight main-sequence and 23 pre-main-sequence variables are found to be part of cluster Stock 8. The main-sequence variables are classified as slow pulsator of the B type, β Cep and δ Scuti stars. Fourteen main-sequence stars could be new class variables as discussed by Mowlavi et al. (2013) and Lata et al. (2014). The age and mass of pre-main-sequence variables are found to be $\lesssim 5$ Myr and in the mass range of 0.5 to 2.8 M_{\odot} , respectively. These pre-main-sequence stars could be T-Tauri variables. We have found 5 and 2 of 23 PMS variables as classical T-Tauri stars and Herbig Ae/Be stars, respectively, whereas 16 PMS stars are classified as weak-line T Tauri stars.

Keywords: Open cluster: Stock 8 – colour–magnitude diagram: Variables: pre-main-sequence stars

1. INTRODUCTION

The study of variable stars is vital to understand the physical properties of stars as well as their circumstellar environment. Therefore, we are pursuing studies of variable stars in young star clusters to study the evolution of pre-main-sequence (PMS) stars. Star clusters are unique laboratories to study the stellar evolution as they provide a sample of stars having approximately the same age, distance, initial composition and spanning range in masses. Additionally, light curves of several stars can be produced simultaneously to identify variable stars among them. Stars on the main-sequence (MS) as well as on the PMS may show variability in their light curves. The brightness may vary in few hours or it may take years.

The largest group of PMS stars is the T Tauri stars (TTSs) (Joy 1945). These TTSs are found along the

Milky Way in star forming regions embedded in gas and dust. The TTSs are slowly contracting to the MS and the location of these stars in the H-R diagram is just above the MS. PMS stars are classified as classical T-Tauri stars (CTTSs), weak-line T-Tauri stars (WTTTSs) (Menard & Bertout 1999) and Herbig Ae/Be (HAeBe) stars. CTTSs are stars with evidence of an accretion disc, whereas WTTTSs have little or no accretion disc. HAeBe stars have relatively higher-mass ($\gtrsim 3 M_{\odot}$) in comparison to TTSs. Most WTTTSs have simple periodic variations, whereas the brightness variations in CTTSs can be complex and irregular (Herbst et al. 1994). Bouvier et al. (1997), Grankin et al. (2007, 2008) and Percy et al. (2010) studied variability in PMS stars. Recently, Lata et al. (2012, 2014) presented light curves of several PMS stars.

Stock 8 ($l=173.371$ deg, $b=-0.183$ deg) is an extremely young stellar open cluster which is located within the HII region IC 417 (Sh2-234) in the Auriga constellation. It contains many OB stars. A detailed study of this

cluster to understand the star formation history, PMS population and the initial mass function (IMF) was presented by Jose et al. (2008). They have determined its fundamental properties such as reddening, distance, age and IMF. The reddening $E(B - V)$ towards the cluster was found to vary between 0.40 to 0.60 mag. The cluster is located at a distance of 2.05 kpc and the radial extent of the cluster is found to be ~ 6 arcmin (~ 3.6 pc). They also identified $H\alpha$ emission and near-infrared (NIR) excess young stellar objects (YSOs) using $H\alpha$ slitless spectroscopy and Two Micron All Sky Survey (2MASS) NIR data, respectively. It is found that the majority of the PMS stars have ages less than 5 Myr, whereas massive stars in the cluster region have an average age of ≤ 2 Myr.

Jose et al. (2017) presented deep VI optical photometry along with JHK and 3.6 and 4.5 μm photometry from UKIDSS and Spitzer-IRAC and studied the stellar content and star formation processes in the young cluster Stock 8. The age of the cluster was estimated as 3 Myr with an age spread of ~ 0.25 Myr. The fraction of YSOs surrounded by disks is found as $\sim 35\%$. Jose et al. (2017) also identified several Class I and Class II YSOs within the Stock 8 region on the basis of color excess in the J , H , K , 3.6, and 4.5 μm bands.

Stock 8, being an extremely young cluster, is an interesting object which contains a number of PMS, O/B type as well as other MS stars. Since the population of variable stars in the region of Stock 8 has not been studied till now, we have carried out time series photometry of the region containing Stock 8 to search for the variable stars. The time series observations of Stock 8 have been taken on 18 nights to find short period variables within the cluster. The observations, procedure of data reduction, identification of variables and determination of period are presented in Section 2. Section 3 deals with the association of variable stars detected in the present work with the cluster Stock 8 on the basis of two colour diagram (TCD) and colour-magnitude diagram (CMD). The estimation of the mass and age of YSOs is described in Section 4. In Section 5, we study the spectral energy distribution of identified YSOs. Identified variables are characterized in Section 6. In section 7, the effect of NIR excess on the rotation period was studied. Section 8 summarizes results obtained in the present study.

2. DATA AND IDENTIFICATION OF VARIABLES

2.1. Observations and Data Reduction

Photometric observations of young open cluster Stock 8 were carried out on a total of 18 nights during 2014 to 2016 from four telescopes. The observations were taken using the 2.4 m Thai National Telescope (TNT) of the

Table 1. Log of optical photometric CCD observations. ‘N’ and ‘Exp.’ refer to number of frames and exposure time respectively.

Date	Filter	(N \times Exp.)	Telescope
12 January 2015	g'	268 \times 13s	2.4 m TNO
13 January 2015	g'	538 \times 13s	2.4 m TNO
14 January 2015	g'	342 \times 13s	2.4 m TNO
08 March 2015	g'	808 \times 13s	2.4 m TNO
10 March 2015	g'	694 \times 13s	2.4 m TNO
06 January 2016	g'	214 \times 13s	2.4 m TNO
10 January 2016	g'	111 \times 13s	2.4 m TNO
01 March 2016	V	83 \times 15s	2.3 HCT
02 March 2016	V	100 \times 13s	2.3 HCT
15 November 2015	V	56 \times 150s	0.5 m TNO
17 November 2015	V	46 \times 90s	0.5 m TNO
19 November 2015	V	47 \times 90s	0.5 m TNO
23 November 2015	V	09 \times 90s	0.5 m TNO
28 November 2015	V	205 \times 90s	0.5 m TNO
29 November 2015	V	84 \times 90s	0.5 m TNO
09 December 2015	V	163 \times 90s	0.5 m TNO
23 December 2014	V	100 \times 60s	1.04 m ARIES
15 January 2015	V	49 \times 60s	1.04 m ARIES

Thai National Observatory (TNO) located on one of the ridges (2457 m) of Doi Inthanon, the highest peak in Thailand. The telescope is equipped with ULTRASPEC which has a 1024 \times 1024 pixel² frame-transfer, electron-multiplying CCD and that together with re-imaging optics provides photometry over a field of 7.7 \times 7.7 arcmin² at frame rates of up to ~ 200 Hz in window mode (for details see Dhillon et al. 2014; Richichi et al. 2014). The observations were taken in g' band on 7 nights during 2015 January 12 to 2016 March 10.

The 0.5 m telescope at TNO was also used for observations of field containing Stock 8. An Andor Tech 2048 \times 2048 pixels CCD camera attached to the 0.5 m Schmidt-Cassegrain Telescope of TNO was used. The plate scale was about 0.684 arcsec/pixel. The resulting field of view of each image was $\sim 23.9 \times 23.9$ arcmin². The observations of Stock 8 were taken in V band from 15 November 2015 to 09 December 2015.

V band photometric imaging of Stock 8 was obtained using the ARIES 1.04 m telescope with a 2k \times 2k CCD. The plate scale of 0.37 arcsec/pixel provides a field of view about 13 arcmin \times 13 arcmin. In order to improve the signal-to-noise ratio (S/N), a 2 \times 2 binning mode was used.

Further, optical observations of Stock 8 region in V band have also been carried out using the 2-m Himalayan Chandra Telescope (HCT) of the Indian Astro-

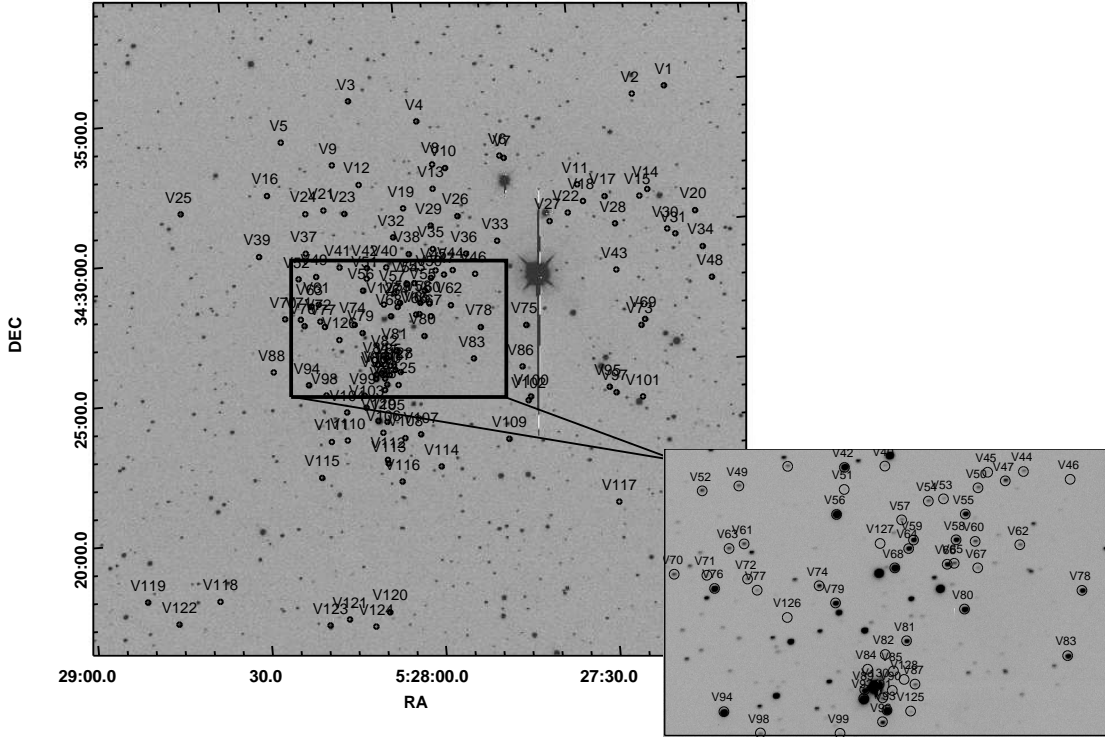


Figure 1. The observed region of Stock 8 in V band. Encircled and labeled with numbers are variable candidates detected in the present study. The equinox J2000.0 is used for equatorial coordinates RA and DEC.

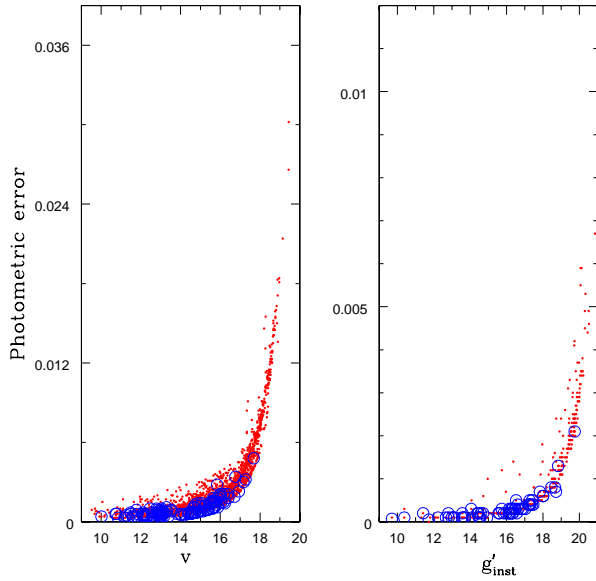


Figure 2. Standard photometric error of all the detected stars. The open circles represent variables identified in the present work. In V band we detected 126 variables, whereas in g' band we detected 64 variables. The total number of detected variables in both bands is 130.

nomical Observatory (IAO) and Himalayan Faint Object Spectrograph Camera (HFOSC). The detector used in the HFOSC is a $2k \times 4k$ SiTe chip with pixel size 15×15 microns. It has plate scale 0.296 arcsec/pixel which gives 10×10 arcmin² field of view.

The observational log is given in Table 1. In total, 3917 frames in the Stock 8 region were secured on 18 nights. We have taken bias and twilight flat images along with the cluster field. Fig. 1 shows the observed region of Stock 8 open cluster. The raw CCD images were preprocessed using Image Reduction and Analysis Facility (IRAF)¹. The pre-processing of images includes bias subtraction, flat fielding and cosmic ray removal. We have used DAOPHOT package (Stetson 1987) to determine the instrumental magnitude of the stars. PSF photometry has been carried out to get the instrumental magnitudes of the sources and it is mainly used for crowded regions to get better results. Details of the procedure can be found in our earlier papers (Lata et al. 2011, 2012).

¹ IRAF is distributed by the National Optical Astronomy Observatory, which is operated by the Association of Universities for Research in Astronomy (AURA) under cooperative agreement with the National Science Foundation.

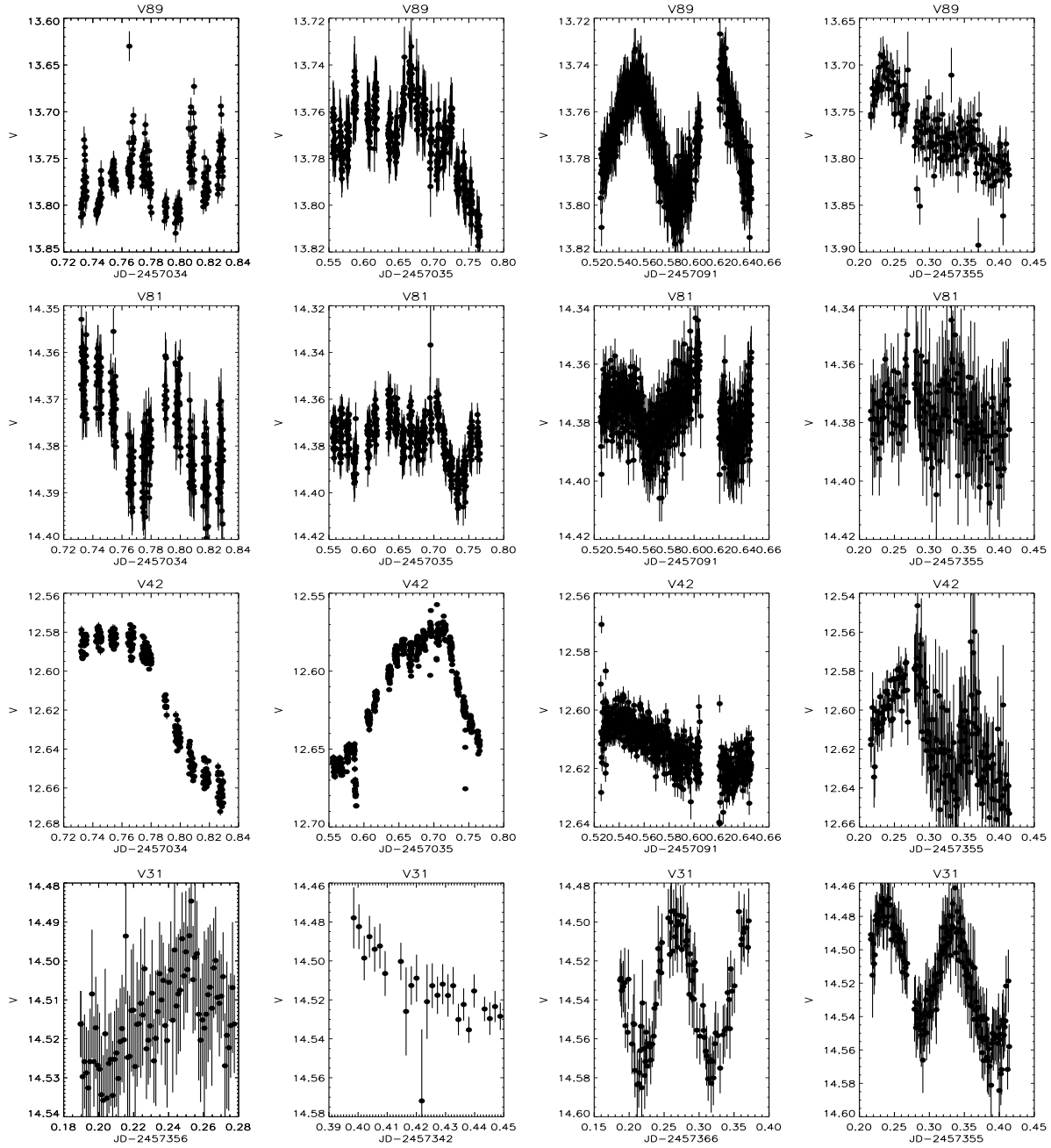


Figure 3. The V band sample light curves of a few variable stars identified in the present work. V represents the standard magnitude in V band.

In order to find the translation, rotation and scaling solutions between different photometry files, we have used DAOMATCH (Stetson 1992). DAOMASTER (Stetson 1992) was used to match the point sources. DAOMASTER uses the output file of DAOMATCH with transformations and a list of photometry files. It refines the transformations using all matched stars and derives robust photometric offsets between frames. We have used DAOMASTER to remove the effects of frame-to-frame flux variation due to airmass and exposure time. This task applies an additive constant in order to make the mean flux level for each frame equal to the reference frame. The corrected magnitudes of each frame were listed in a *.cor* file. We have *.cor* files for *V* and *g'* bands. The *V* band *.cor* contains 1721 sources while *g'* *.cor* has 361 stars. These corrected instrumental magnitudes of stars are further transformed into standard ones in the next section.

Fig. 2 shows the photometric error of all the stars and identified variables as a function of mean *v* and g'_{inst} instrumental magnitude. The standard photometric error of the mean magnitude for each star, based on photometric error of individual frame, has been taken from the *.mag* file given by the DAOMASTER. Out of 130 stars, only 126 are plotted in the left panel of Fig. 2. Four stars could not be detected in observations taken in *V* band. Right panel of Fig. 2 displays 64 variables which were detected in *g'* band. The standard photometric error of mean magnitude in *g'* band is found to be much smaller than that of *V* band as shown in Fig. 2. This could be due to large number of observations in *g'* band compared to those in *V* band.

2.2. Archival data

The *UBVI* data of Stock 8 have been taken from Jose et al. (2008, 2017), whereas the NIR data have been taken from the 2MASS Point Source Catalogues (PSC; Cutri et al. 2003). The 2MASS counterparts of the variables were searched using a match value of 3 arc-sec. The 2MASS magnitudes and colours were transformed to the Caltech (CIT) photometric system using the relations given on the 2MASS web site². We have also used NASA's Wide-field Infrared Survey Explorer (WISE) data (Cutri et al. 2012) taken at wavelengths 3.4, 4.6, 12.0, and 22.0 μm .

2.3. Transformation, identification of variable and determination of period

The corrected *v* instrumental magnitudes of variables were converted into standard ones by obtaining trans-

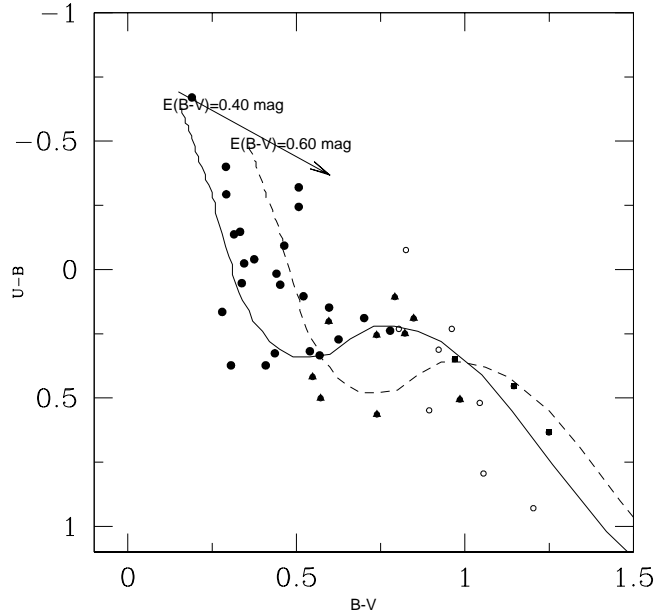


Figure 4. $(U - B)/(B - V)$ TCD for variables detected in the present work. The *UBV* data are taken from Jose et al. (2008). The continuous and dashed curve represent the zero-age-main-sequence (ZAMS) (Girardi et al. 2002) which are moved in the direction of the reddening vector for reddening $E(B - V) = 0.4$ mag and 0.60 mag. Filled and open circles represent MS and field/unclassified variables, respectively. Filled squares and triangles show PMS and BP population stars, respectively. The straight line indicates reddening vector for $E(U - B)/E(B - V) = 0.72$.

Table 2. The sample of data for the variable stars. The complete data of all the variable stars are available in electronic form.

ID	JD	V (mag)	σ_V (mag)
V1	2457355.2165970	12.880	0.021
V1	2457355.2187500	12.874	0.022
V1	2457355.2208910	12.893	0.019
V1	2457355.2230440	12.878	0.020
...
...
...
...

formation equation using the photometric data for the region by Jose et al. (2008). The following transformation equation was used to convert present *v* magnitudes into standards ones.

$$V = (0.965 \pm 0.01) \times v + 1.453 \pm 0.022 \quad (1)$$

² <http://www.astro.caltech.edu/~jmc/2mass/v3/transformations/>

Table 3. The photometric data, period, amplitude, time of maximum brightness T_0 and classification of 130 variables in the region of Stock 8. The $UBVI$ and NIR data have been taken from Jose et al. (2008, 2017) and 2MASS point source catalogue (Cutri et al. 2003), respectively. Column 15 infers classification (c1) of stars as per Jose et al. (2017), while column 16 shows present classification (c2) of variables.

ID	RA(2000)	Dec(2000)	V (mag)	$U - B$ (mag)	$B - V$ (mag)	$V - I$ (mag)	J (mag)	H (mag)	K (mag)	Period (days)	Amp. (amp)	T_0 (2457000.+)	prob.	c1	c2
V1	81.808528	34.582028	-	-	-	-	-	-	-	0.174048	0.027	355.344271	0.15	-	unclass.
V2	81.832167	34.578667	-	-	-	-	-	-	-	0.205270	0.093	355.411887	1.	-	unclass.
V3	82.037417	34.587694	-	-	-	-	11.155	10.577	10.446	0.218461	0.034	355.314306	0.	-	Field
V4	81.989389	34.5725	-	-	-	-	-	-	-	0.232714	0.025	366.241551	0.99	-	unclass.
V5	82.088444	34.56625	16.583	-	0.998	1.125	14.702	14.275	14.188	0.262154	0.123	356.201551	1.	-	BP
V6	81.931556	34.548167	-	-	-	-	-	-	-	0.250823	0.067	355.218750	1.	-	unclass.
V7	81.9285	34.546583	-	-	-	-	-	-	-	0.341004	0.037	350.175995	1.	-	unclass.
V8	81.980583	34.546111	-	-	-	-	-	-	-	0.363382	0.130	350.175995	1.	-	unclass.
V9	82.052972	34.550306	16.952	-	0.981	1.209	14.884	14.34	14.278	0.387657	0.158	356.201551	1.	-	Field
V10	81.9715	34.543333	-	-	-	-	-	-	-	0.232714	0.023	366.241551	1.	-	unclass.
V11	81.877167	34.527278	-	-	-	-	-	-	-	0.352351	0.128	350.175995	1.	-	unclass.
V12	82.034833	34.537361	16.655	-	1.192	1.28	14.461	13.908	13.814	0.377979	0.116	015.372340	1.	-	Field
V13	81.981722	34.531611	-	-	-	-	-	-	-	0.203531	0.056	355.218750	1.	-	unclass.
V14	81.826944	34.521111	-	-	-	-	-	-	-	0.372874	0.121	344.233750	0.18	-	unclass.
V15	81.833083	34.517556	-	-	-	-	-	-	-	0.267183	0.100	355.223044	1.	-	unclass.
V16	82.101611	34.535111	15.82	0.19	0.848	1.001	14.167	13.784	13.724	0.377563	0.096	350.177106	1.	-	BP
V17	81.858194	34.518917	-	-	-	-	-	-	-	0.484089	0.040	366.219016	1.	-	unclass.
V18	81.874056	34.517083	-	-	-	-	-	-	-	0.267183	0.082	356.276539	1.	-	unclass.
V19	82.004222	34.521333	16.64	-	2.036	2.326	12.604	11.737	11.426	0.377159	0.128	356.204769	1.	-	PMS(WTTS)
V20	81.793806	34.506194	-	-	-	-	-	-	-	0.319554	0.019	346.320949	0.	-	unclass.
V21	82.061806	34.523806	16.568	-	0.858	1.112	14.716	14.431	14.225	0.376725	0.104	356.205845	1.	-	BP
V22	81.885722	34.510944	-	-	-	-	-	-	-	0.296789	0.049	350.175995	1.	-	unclass.
V23	82.046917	34.520806	12.892	0.318	0.54	0.661	11.743	11.56	11.49	0.170225	0.036	366.219016	1.	-	MS(new class)
V24	82.075056	34.522472	16.607	-	0.928	1.088	14.786	14.349	14.193	0.377979	0.094	356.205845	1.	-	BP
V25	82.164944	34.52825	13.878	0.929	1.203	1.258	11.481	10.907	10.751	0.179500	0.035	342.389525	0.41	-	Field
V26	81.965528	34.514111	-	-	-	-	9.075	8.441	8.219	0.363838	0.082	366.241551	1.	-	PMS(WTTS)
V27	81.899333	34.506722	-	-	-	-	-	-	-	0.228593	0.050	350.177106	1.	-	unclass.
V28	81.852306	34.502222	-	-	-	-	-	-	-	0.295748	0.022	342.393125	0.04	-	unclass.
V29	81.985389	34.509778	13.333	-	-	0.902	11.846	11.581	11.477	0.260328	0.037	355.318600	1.	-	MS
V30	81.815028	34.496639	-	-	-	-	-	-	-	0.210166	0.109	356.271169	1.	-	Field
V31	81.8095	34.493333	-	-	-	-	-	-	-	0.112561	0.042	350.177106	1.	-	δ Scuti?
V32	82.013194	34.504528	13.363	-	6.442	3.604	7.124	5.671	4.75	0.352105	0.040	355.362512	1.	-	Field
V33	81.938389	34.497556	-	-	-	-	-	-	-	0.420986	0.099	344.198507	1.	-	unclass.
V34	81.790556	34.484417	-	-	-	-	-	-	-	0.281200	0.022	366.266817	0.01	-	unclass.
V35	81.985278	34.495722	16.685	-	1.254	1.524	14.1	13.525	13.308	0.144190	0.065	034.828316	1.	-	Field
V36	81.961611	34.491361	-	-	-	-	12.109	11.948	11.79	0.127839	0.092	036.828517	1.	-	Field
V37	82.077139	34.498917	16.368	-	1.788	2.426	12.254	11.417	11.148	0.427844	0.093	449.265729	1.	-	PMS(WTTS)
V38	82.002917	34.493806	12.629	0.148	0.597	0.643	11.287	11.013	10.954	0.052942	0.024	089.636788	1.	-	MS(SPB)
V39	82.110972	34.499111	15.385	0.249	0.822	1.06	13.605	13.202	13.121	0.267509	0.034	350.175995	1.	-	BP
V40	82.019944	34.486944	16.667	-	0.973	1.059	14.984	14.587	14.518	0.307807	0.097	038.167660	1.	-	BP
V41	82.053556	34.489083	15.878	-	0.837	1.148	13.828	13.427	13.291	0.182051	0.018	036.830146	1.	-	BP
V42	82.033972	34.487472	12.665	-0.293	0.292	0.479	11.859	11.744	11.626	0.189434	0.031	036.829257	1.	-	MS(SPB)
V43	81.85425	34.474667	-	-	-	-	-	-	-	0.180579	0.060	355.230556	1.	-	unclass.
V44	81.972194	34.482222	16.084	-	0.891	1.173	14.109	13.697	13.662	0.230325	0.059	089.632938	1.	-	BP
V45	81.984583	34.482833	17.323	-	1.733	2.281	13.383	12.536	12.209	0.498848	0.239	038.339120	1.	-	PMS(WTTS)
V46	81.956278	34.478917	-	-	-	-	-	-	-	0.549653	0.408	015.281560	1.	-	unclass.
V47	81.97875	34.479972	15.143	0.107	0.792	0.987	13.469	13.14	13.037	0.144650	0.060	036.828517	1.	-	BP
V48	81.785833	34.465722	-	-	-	-	-	-	-	0.220069	0.026	355.314306	0.	-	unclass.
V49	82.071028	34.484583	15.605	0.519	1.044	1.346	13.275	12.823	12.666	0.128532	0.024	091.620475	1.	-	Field
V50	81.988389	34.478611	15.715	0.231	0.804	0.906	14.04	13.75	13.612	0.048021	0.047	091.645200	1.	-	Field
V51	82.034694	34.481194	17.773	-	1.388	1.668	14.861	14.177	13.91	0.168994	0.041	091.638094	1.	-	PMS(WTTS)
V52	82.083833	34.484028	15.416	0.501	0.572	0.921	13.789	13.574	13.415	0.114324	0.026	091.620475	1.	-	BP
V53	82.000639	34.47625	16.679	-	0.98	1.149	14.761	14.309	14.227	0.334858	0.047	036.820481	1.	-	BP
V54	82.005944	34.475944	15.825	0.564	0.739	0.986	14.098	13.775	13.62	0.234592	0.022	036.831182	1.	-	BP
V55	81.993556	34.471389	13.934	0.272	0.625	0.795	12.577	12.323	12.246	0.120563	0.035	036.828517	1.	-	MS(new class)
V56	82.038083	34.474222	11.888	-0.4	0.291	0.479	11.069	10.948	10.907	0.252462	0.019	355.362512	1.	III/field	MS(SPB)
V57	82.015722	34.471194	16.077	-	1.075	1.409	13.55	13.181	12.95	0.224849	0.017	036.820629	0.99	III/field	Field
V58	81.9975	34.46425	13.978	0.794	1.055	1.256	11.87	11.29	11.178	0.141626	0.028	036.828517	1.	III/field	Field
V59	82.012194	34.465167	14.08	-0.093	0.464	0.702	12.834	12.592	12.479	0.364331	0.014	036.829405	1.	III/field	MS(new class)
V60	81.990944	34.463361	15.491	0.312	0.922	1.078	13.647	13.243	13.147	0.166027	0.023	089.635751	0.93	III/field	Field
V61	82.070889	34.467917	15.565	0.634	1.249	1.568	12.755	11.93	11.433	0.128722	0.026	089.560241	1.	-	PMS(CTTS)
V62	81.975611	34.461389	15.82	0.506	0.985	1.095	13.884	13.463	13.334	0.145872	0.046	036.820481	0.95	-	BP
V63	82.076222	34.466944	15.66	0.255	0.738	1.075	13.93	13.529	13.444	0.113297	0.025	089.558021	0.85	-	BP
V64	82.014139	34.462833	14.042	0.059	0.452	0.662	12.784	12.493	12.363	0.196151	0.010	366.241551	1.	III/field	MS(new class)
V65	81.998833	34.457583	15.719	0.202	0.596	1.026	14.103	13.756	13.702	0.229548	0.011	355.218750	1.	III/field	BP
V66	82.001278	34.457472	14.178	0.373	0.409	0.491	13.292	13.174	13.095	0.094072	0.014	089.531074	1.	III/field	MS(δ Scuti)
V67	81.990833	34.45575	16.418	-	0.926	1.098	14.567	14.106	14.006	0.180390	0.014	366.259306	1.	III/field	BP
V68	82.0195	34.457639	12.229	0.189	0.701	0.862	10.774	10.436	10.322	0.216378	0.040	035.754519	1.	III/field	MS(SPB)
V69	81.836583	34.443833	-	-	-	-	-	-	-	0.273521	0.023	366.293657	0.99	-	unclass.
V70	82.095944	34.460833	15.495	0.231	0.961	1.151	13.505	13.099	12.94	0.114027	0.034	450.124711	1.	-	Field
V71	82.084667	34.459806	16.618	-	0.866	1.09	14.826	14.374	14.259	0.093118	0.026	366.211505	1.	-	BP
V72	82.070722	34.457806	16.286	-	0.813	1.035	14.573	14.218	14.033	0.120263	0.024	089.559353	1.	III/field	BP
V73	81.839556	34.440472	-	-	-	-	-	-	-	0.254942	0.022	366.241551	1.	-	unclass.
V74	82.046167	34.45425	14.961	-	1.632	1.782	11.832	11.065	10.834	0.147866	0.030	089.559797	0.01	III/field	PMS(WTTS)
V75	81.922556	34.446028	-	-	-	-	11.06	10.958	10.903	0.267183	0.066	355.364664	1.	-	Field
V76	82.082389	34.455861	12.806	0.373	0.306	0.41	12.078	11.987	11.942	0.111308	0.025	089.559353	1.	-	MS(δ Scuti)
V77	82.067722	34.454389	16.281	-	1.904	2.189	12.445	11.541	11.249	0.249165	0.036	089.637232	0.91	III	

Table 3. Continued

ID	RA(2000)	Dec(2000)	V (mag)	$U - B$ (mag)	$B - V$ (mag)	$V - I$ (mag)	J (mag)	H (mag)	K (mag)	Period (days)	Amp. (amp)	T_0 (2457000.+)	prob.	c1	c2
V79	82.041	34.448972	13.717	0.053	0.338	0.512	12.816	12.715	12.621	0.183882	0.028	089.545288	1.	III/field	MS(new class)
V80	81.996611	34.444278	13.211	0.165	0.28	0.411	12.459	12.283	12.26	0.128475	0.021	036.828665	1.	III/field	MS(new class)
V81	82.017556	34.436556	14.397	0.334	0.569	0.72	13.219	13.002	12.774	0.063815	0.010	089.559945	1.	III/field	MS(new class)
V82	82.025333	34.433111	17.244	-	1.103	1.62	14.352	13.732	13.503	0.171297	0.047	355.407593	1.	III/field	PMS(WTTS)
V83	81.962333	34.428611	13.963	-0.076	0.825	0.92	12.329	12.098	11.981	0.123067	0.042	089.631309	0.0	-	Field
V84	82.031833	34.429306	17.633	-	-	1.711	14.566	13.9	13.602	0.352718	0.304	342.382350	1.	III/field	PMS(WTTS)
V85	82.022972	34.428222	16.91	-	1.138	1.557	14.414	13.761	13.522	0.144094	0.075	089.530482	1.	III/field	PMS(WTTS)
V86	81.927806	34.421528	-	-	-	-	12.303	12.011	11.916	0.377563	0.026	366.241551	1.	-	Field
V87	82.015917	34.423972	15.715	0.454	1.145	1.421	13.233	12.639	12.422	0.306247	0.023	036.828665	1.	III/field	PMS(WTTS)
V88	82.107361	34.42975	18.788	-	1.219	1.995	15.236	14.771	14.388	0.250687	0.429	342.441620	1.	-	Field
V89	82.033444	34.4235	13.891	-	-	1.011	12.162	11.854	11.717	0.064978	0.018	036.723177	1.	III/field	Field
V90	82.023944	34.422694	16.85	-	-	1.74	13.949	13.237	12.975	0.095051	0.157	355.400081	1.	III/field	PMS(WTTS)
V91	82.027472	34.420778	15.901	-	-	1.61	13.325	12.551	12.414	0.164707	0.072	089.531074	0.21	III/field	PMS(WTTS)
V92	82.034056	34.421028	11.048	-	-	0.325	10.514	10.469	10.449	0.173359	0.029	035.648077	1.	III/field	MS
V93	82.026361	34.417194	12.326	0.326	0.436	0.628	11.122	10.807	10.703	0.158525	0.024	089.549877	1.	III/field	MS(new class)
V94	82.08275	34.420444	12.19	-0.244	0.507	0.754	10.876	10.689	10.606	0.184804	0.020	355.364664	1.	III/field	MS(SPB)
V95	81.86625	34.405194	-	-	-	-	-	-	-	0.392364	0.020	342.393125	0.99	-	unclass.
V96	82.02825	34.413972	14.8	0.349	0.97	1.285	12.44	11.693	11.055	0.158525	0.050	089.560537	1.	III/field	PMS(HAeBe)
V97	81.86175	34.401583	-	-	-	-	-	-	-	0.396248	0.038	366.207211	1.	-	unclass.
V98	82.07075	34.413528	15.935	-	1.051	1.341	13.545	12.897	12.431	0.120824	0.042	089.559353	1.	II	PMS(HAeBe)
V99	82.04325	34.411611	16.825	-	1.52	1.892	13.519	12.569	12.042	0.179223	0.055	089.636343	1.	III/field	PMS(CTTS)
V100	81.9235	34.403194	-	-	-	-	11.629	11.349	11.245	0.220333	0.018	366.326933	1.	-	Field
V101	81.842917	34.397806	-	-	-	-	-	-	-	0.352334	0.254	342.412882	1.	-	unclass.
V102	81.9255	34.401083	14.168	-	-	0.972	12.567	12.293	12.212	0.272409	0.024	346.336366	1.	-	MS
V103	82.042639	34.404361	13.124	0.104	0.521	0.776	11.75	11.537	11.399	0.279487	0.040	089.589409	0.51	III/field	MS(new class)
V104	82.056917	34.402444	14.984	0.548	0.894	1.204	12.863	12.457	12.262	0.112132	0.013	346.331956	0.	III/field	Field
V105	82.028472	34.394944	13.361	-0.137	0.315	0.508	12.523	12.426	12.362	0.161072	0.028	089.559353	1.	III/field	MS(new class)
V106	82.032056	34.388639	17.108	-	1.315	1.681	14.256	13.611	13.308	0.229596	0.038	355.221968	1.	III/field	PMS(CTTS)
V107	82.005	34.385944	13.291	-0.024	0.345	0.482	12.333	12.204	12.158	0.069255	0.008	089.612358	1.	III/field	MS(new class)
V108	82.016528	34.384417	15.183	0.418	0.548	0.721	13.82	13.508	13.352	0.199593	0.012	036.811076	0.	III/field	BP
V109	81.94175	34.379028	12.427	-0.32	0.507	0.732	11.147	10.993	10.923	0.195896	0.020	355.294988	1.	-	MS(SPB)
V110	82.058139	34.385722	18.627	-	-	1.828	15.351	14.699	14.396	0.648860	0.412	356.251852	1.	III/field	PMS(CTTS)
V111	82.069722	34.385583	16.519	-	1.153	1.246	14.419	13.856	13.745	0.102806	0.034	036.821073	1.	-	Field
V112	82.030417	34.372306	16.756	-	-	1.195	14.475	14.066	13.886	0.171350	0.047	036.829405	1.	-	BP
V113	82.030139	34.370111	13.922	-	1.957	2.189	10.05	9.1	8.81	0.130534	0.013	355.294988	0.	-	PMS(WTTS)
V114	81.992139	34.365833	13.629	-0.04	0.375	0.556	12.675	12.55	12.494	0.176857	0.015	366.294722	1.	-	MS(new class)
V115	82.078833	34.364639	13.705	-	-	1.144	11.708	11.232	11.111	0.275857	0.031	038.347990	0.	-	Field
V116	82.021194	34.358694	13.329	-0.147	0.333	0.506	12.429	12.346	12.241	0.450141	0.039	355.294988	1.	-	MS(SPB)
V117	81.8665	34.336306	-	-	-	-	15.142	14.617	14.353	0.187340	0.210	356.273322	1.	-	Field
V118	82.1595	34.295611	-	-	-	-	14.558	14.155	13.98	0.053956	0.068	355.357141	1.	-	Field
V119	82.211611	34.298583	-	-	-	-	11.545	11.381	11.313	0.050593	0.028	356.214433	1.	-	Field
V120	82.038111	34.281444	13.214	0.016	0.441	0.645	12.089	11.948	11.834	0.140128	0.015	355.372176	0.	-	MS(new class)
V121	82.067417	34.279028	14.276	0.238	0.778	0.924	12.769	12.475	12.368	0.140456	0.027	346.331956	0.	-	MS(new class)
V122	82.190361	34.283972	-	-	-	-	12.053	11.883	11.819	0.249029	0.043	356.228380	1.	-	Field
V123	82.081778	34.276417	-	-	-	-	11.736	11.602	11.551	0.311387	0.049	356.216574	1.	-	Field
V124	82.048889	34.273556	15.861	-	1.15	1.19	13.857	13.361	13.217	0.295529	0.039	355.375394	0.97	-	BP
V125	82.018222	34.416361	17.827	-	1.389	1.779	14.975	13.853	13.131	0.501000	0.360	035.695247	1.	II	PMS(CTTS)
V126	82.058111	34.445917	17.866	-	1.069	1.421	15.585	14.954	14.7	0.452000	0.116	036.821073	1.	III/field	PMS(WTTS)
V127	82.023861	34.464944	18.877	-	-	1.641	16.052	15.706	15.065	0.446000	0.195	091.643424	1.	III/field	Field
V128	82.019528	34.425556	18.441	-	-	1.911	15.499	14.653	14.422	0.315000	0.456	089.530926	1.	unknown	PMS(WTTS)
V129	82.034903	34.395958	10.149	-	-	0.387	9.317	9.256	9.231	0.229000	0.164	089.632198	1.	unknown	MS
V130	82.029761	34.424144	8.953	-0.67	0.19	0.282	8.378	8.358	8.324	0.169000	0.381	036.715420	1.	unknown	MS(β Cep)

Table 4. Mass and age of probable PMS stars.

ID	Mass(CMD) (M_{\odot})	Age(CMD) (Myr)	Mass(SED) (M_{\odot})	Age(SED) (Myr)
V19	0.69±0.02	<=0.10±0.01	-	-
V26	-	-	-	-
V37	0.75±0.02	<=0.10±0.01	-	-
V45	0.55±0.03	0.16±0.04	-	-
V51	1.32±0.03	4.36±0.67	1.23 ± 0.50	4.21± 2.30
V61	2.01±0.10	0.64±0.10	2.71 ± 1.00	3.21± 2.10
V74	1.56±0.08	0.20±0.02	3.67 ± 0.14	0.93± 1.42
V77	0.79±0.02	<=0.10±0.01	1.01 ± 0.41	1.22± 0.35
V82	1.44±0.05	2.64±0.44	2.45 ± 0.60	6.35± 2.31
V84	1.25±0.06	2.72±0.49	-	-
V85	1.63±0.04	2.54±0.34	-	-
V87	2.32±0.05	1.49±0.31	1.88 ± 0.52	1.85± 1.74
V90	1.20±0.07	0.92±0.14	-	-
V91	1.73±0.09	0.69±0.09	-	-
V96	2.75±0.15	1.92±0.46	5.68 ± 0.51	4.15± 1.43
V98	2.13±0.08	3.15±0.67	3.41 ± 0.29	6.39± 2.71
V99	0.93±0.05	0.52±0.05	2.47 ± 1.04	3.74± 2.20
V106	1.33±0.07	1.64±0.26	1.95 ± 0.90	4.13± 3.30
*V110	1.04±0.04	5.82±1.01	-	-
V113	2.20±0.02	0.01±0.01	-	-
V125	1.11±0.06	2.43±0.41	2.59 ± 1.37	0.49± 0.98
V126	1.29±0.01	>10 -	1.83 ± 0.35	0.28± 0.12
V128	0.91±0.05	2.85±0.48	-	-

where V and v are standard and instrumental magnitude, respectively.

The g' band instrumental magnitude was converted into V band standard magnitude using the following transformation equation

$$V = (0.912 \pm 0.021) \times g'_{inst} + 0.79 \pm 0.032 \quad (2)$$

We could not use colour term in the transformation equations as time series photometry for two colours was not available. However, to check the effect of colour term on transformation, we used average v magnitude from present time series observations and converted to standard magnitude using the following equation

$$V - v = (-0.079 \pm 0.012) \times (V - I) + (1.085 \pm 0.017) \quad (3)$$

where V and $(V - I)$ colours are taken from Jose et al. (2008). We have found that the effect of colour term in one magnitude bin is negligible. Since in the present study the amplitude is less than one magnitude, it will have no effect on light curves of variable stars.

The light curves of all the cross matched stars by the DAOMASTER were generated by plotting standard V magnitudes of stars against Julian date (JD). We visually checked the light curves of all the 1721 stars. A star has been selected as variable star if it showed brightness variation of at least ~ 0.01 mag. The present study did

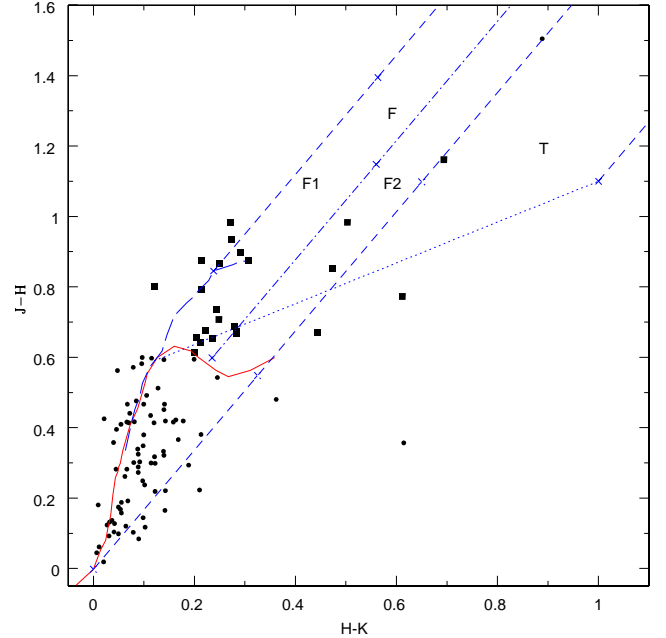


Figure 5. $(J - H)/(H - K)$ TCD for variables identified in the field of Stock 8. JHK data are taken from the 2MASS catalogue (Cutri et al. 2003). The continuous and long dashed curve show sequences for dwarfs and giants (Bessell & Brett 1988), respectively. The locus of TTSs (Meyer et al. 1997) is represented by dotted curve. The reddening vectors (Cohen et al. 1981) are shown by small dashed lines and an increment of visual extinction of $A_V = 5$ mag is denoted by crosses on the reddening vectors. The ‘F’ region and ‘T’ region are mentioned in Section 3, where the sub-regions ‘F1’ and ‘F2’ are discussed in Section 6.2. Filled squares and circles represent PMS and other (MS, BP, field/unclassified) variables, respectively.

not use RMS dispersion criterion as this criterion may not be able to detect small amplitude periodic variables. Hence, the probable variables were identified visually by inspecting their light curves. The visual inspection yields 130 variable candidates in the field of Stock 8. The sample light curves of a few variables are shown in Fig. 3. The sample of data for variables is given in Table 2. The complete table is available in electronic form. The variable candidates identified in the present work are marked in Fig. 1. The variability of variable stars was also checked using the χ^2 test (Sesar et al. 2007). Out of 130 variables discovered, 112 have probability $\geq 90\%$. Visual inspection of the remaining variables reveals a significant variability, hence we also considered them suspected variables. The identification number, coordinates and optical as well as photometric data in NIR of the identified variables are listed in Table 3. To convert CCD pixel coordinates of the identified variables to their celestial coordinates (RA and DEC) for

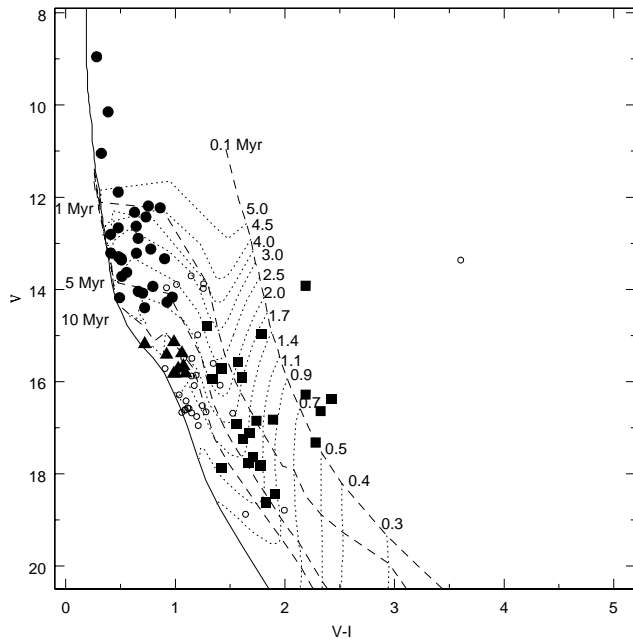


Figure 6. $V/(V - I)$ CMD for variable stars detected in the cluster Stock 8. The V and I data are taken from Jose et al. (2008). The filled squares represent probable TTSS, whereas filled circles, open circles and filled triangles show MS stars, field/unclassified and BP population in the direction of the cluster, respectively. The continuous curve shows ZAMS by Girardi et al. (2002) while dashed lines represent PMS isochrones for 0.1, 1, 5, 10 Myrs (Siess et al. 2000). The PMS evolutionary tracks of stars for different masses taken from Siess et al. (2000) are shown by dotted curves.

J2000 we have used the CCMAP and CCTRAN tasks available in IRAF.

The Lomb-Scargle periodogram (Lomb 1976; Scargle 1982) has been used to determine the probable periods of variable stars. This periodogram gives better results even when data are taken at irregular intervals. The periods were further confirmed using the NASA exoplanet archive periodogram service. The phased light curves were visually inspected, and we have considered the period which shows the best phased light curve. We have listed the most probable periods of the stars with their amplitudes in Table 3. The folding of light curves for variable stars are done with their estimated periods. The phased light curves will be further discussed in Section 6.

3. IDENTIFICATION OF PROBABLE MEMBERS OF STOCK 8

The $V/(V - I)$ CMD of the cluster region by Jose et al. (2008, cf. their figure 8b and 8c) clearly reveals contamination due to field star population. Ninety and

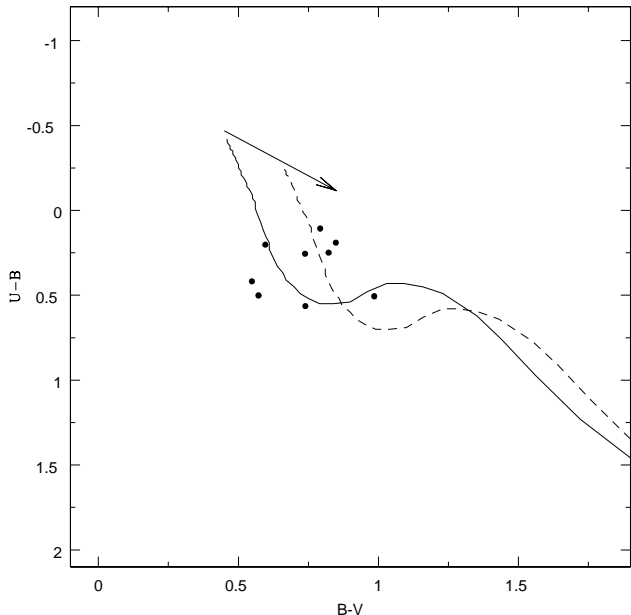


Figure 7. $(U - B)/(B - V)$ TCD for variables associated with the BP population. The UBV photometric data are taken from Jose et al. (2008). The continuous and dashed curve show the ZAMS by Girardi et al. (2002) which are moved in the direction of the reddening vector for reddening $E(B - V) = 0.70$ mag and 0.90 mag. The straight line indicates reddening vector for $E(U - B)/E(B - V) = 0.72$.

39 of the 130 variables identified in the present work are found to be common with those reported by Jose et al. (2008) and (2017), respectively. All the 39 variables (Jose et al. 2017) are included in the data by Jose et al. (2008). The individual membership of these 90 stars was not discussed by Jose et al. (2008). Their figure 8d represents statistically cleaned CMD of the cluster. Hence, we have used $(U - B)/(B - V)$, NIR $(J - H)/(H - K)$ TCDs and $V/(V - I)$ CMD to find out the association of the identified variables with the cluster.

The $(U - B)/(B - V)$ TCD for 44 variable candidates is shown in Fig. 4 as $(U - B)$ colours are available for only 44 variables. The distribution of MS variables in Fig. 4 reveals a variable reddening in the cluster region with the reddening value of $E(B - V)_{min} = 0.40$ mag. The sources lying within the MS band having $E(B - V) = 0.4$ mag to 0.6 mag with spectral type from O to A can be considered as possible MS members of the cluster. Fig. 5 shows $(J - H)/(H - K)$ TCD of 101 variables as the JHK counterparts for 29 variables could not be detected. The YSOs either show significant amount of $H\alpha$ emission and/or NIR excess. Therefore, the $(J - H)/(H - K)$ TCD is a very useful tool to identify YSOs. In Fig. 5, the sources lying in ‘F’ region could be

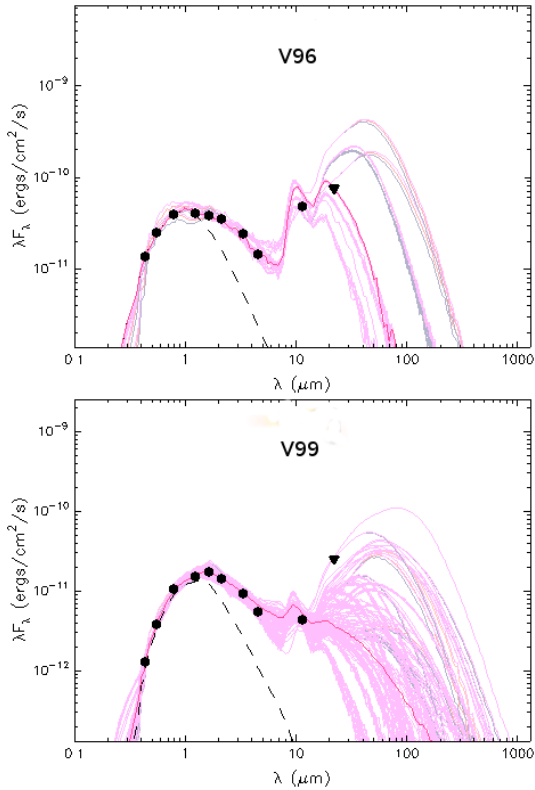


Figure 8. SEDs of the YSOs V96 and V99. The dark line shows the best fit model, and the light pink lines show subsequent models that satisfy $\chi^2 - \chi_{\min}^2 \leq 2N_{\text{data}}$ criterion. The dashed line represents the best fit model for the stellar photosphere of central source. The observed flux values are represented by filled circles. The $22 \mu\text{m}$ flux is shown by triangle, which is considered as upper limit while fitting the model.

either field stars or Class III and Class II sources with small NIR excesses. The sources lying in the ‘T’ region can be considered mostly as CTTSs (Class II objects).

Fig. 6 shows the $V/(V - I)$ CMD for 90 variables as $(V - I)$ colour for remaining 40 variables was not available. We have plotted a theoretical isochrone of 4 Myr for $Z=0.02$ (Girardi et al. 2002) with continuous curve in Fig 6. Fig. 6 also plots the PMS isochrones and evolutionary tracks for various ages and various masses (Siess et al. 2000), respectively. The distance (2.05 kpc) and minimum reddening $E(V - I)_{\min} = 0.5$ mag have been used to correct all the isochrones and evolutionary tracks. The $E(V - I)_{\min}$ has been estimated using the relations $E(V - I)/E(B - V) = 1.25$ mag and $E(B - V) = 0.40$ mag.

Based on the above mentioned TCDs and CMD, we have established membership of 51 stars (28 MS and 23 PMS stars). Of the remaining 79 stars, 29 variables remained unclassified due to unavailability of their photometric and NIR data. Fifty stars may belong to the

field star population. Twenty one out of these 50 stars are found to be distributed below the 10 Myr isochrone around $(V - I) \sim 1.2$ mag and $V \sim 15.6$ to 17.0 mag. This population may belong to the blue plume (BP) of Norma-Cygnus arm as discussed by Jose et al. (2008). $U - B$ colour is available for 9 of these 50 variables. The location of these 9 variables in $U - B/B - V$ diagram (Fig. 7) indicates that these stars have $E(B - V)$ in the range of 0.7-0.9 mag, comparable to the BP Population of Norma-Cygnus arm (see e.g. Pandey et al. 2006 and Jose et al. 2008). Hence, we consider these 9 variable stars as of the BP population. The classification of variables detected in the present work is given in the last column of Table 3.

4. AGE AND MASS ESTIMATION

The ages and masses of PMS stars have been estimated by comparing present observations with the theoretical models to study the evolution of amplitude and period of PMS stars. For this, we have used $V/V - I$ CMD and PMS isochrones by Siess et al. (2000). The PMS isochrones of Siess et al. (2000) in the age range of 0.1 to 10 Myr with an interval of 0.1 Myr have been used. We then interpolated these isochrones to make more continuous curves. These theoretical isochrones of Siess et al. (2000) corrected for the distance (2.05 kpc) and reddening ($E(V - I)_{\min} = 0.5$) have been compared with the location of PMS stars in the $V/V - I$ CMD. Finally, we determine the age and mass of the PMS star corresponding to the closest isochrone on the CMD. Thus, the estimated age and mass may be affected by random errors in observations, errors in transformation to the standard system and systematic errors because of using different theoretical evolutionary tracks. We presume that the systematic errors do not have any effect on the mass and age estimates obtained in the present work as we are using the model by Siess et al. (2000) for all the PMS stars. Assuming normal error distribution and using the Monte Carlo simulations (see e.g., Chauhan et al. 2009) the random errors were propagated to the observed estimates of $V/(V - I)$ and $E(V - I)$ to estimate the random errors in the determination of mass and age. Another source of error may be the presence of binaries. A star will become brighter in the presence of binary which, consequently, will yield a younger age. For equal mass binary, the expected error in the estimation of age of PMS stars is ~ 50 to 60%. Since we do not know the fraction of binaries in the Stock 8 cluster, it is difficult to determine the effect of binaries on the estimation of mean age. However, the study of Duquennoy & Mayor (1991) of multiplicity among solar type stars in the solar neighbourhood suggests that the distribution

of mass ratio ($M1/M2$) shows a peak around ~ 0.23 . If the binaries in Stock 8 cluster have a similar mass distribution, the effect of binaries on age estimates may not be significant. The age and mass estimates of the YSOs are in the range of 0.2 to 5.8 Myr and ~ 0.5 to $\sim 2.75 M_{\odot}$, respectively, which are comparable with the ages and masses of TTSS. The age spread of YSOs in the Stock 8 region indicates a non-coeval star formation in the region. The estimated ages and masses along with their errors are given in Table 4.

5. SPECTRAL ENERGY DISTRIBUTION

The spectral energy distribution (SED) of YSOs is a useful tool to characterize the circumstellar disk properties of YSOs. To construct the SEDs of YSOs we have used Robitaille et al. (2006, 2007) models for radiative transfer and multiwavelength i.e., optical (BVI), NIR (JHK) and WISE (3.4, 4.6, 12.0, and 22.0 μm) data. The 22 μm data have been used as upper limit because of its large beam (~ 22 arcsec) and crowding of the region. To fit the SED models we have taken distance to the cluster as 2.05 ± 0.10 kpc and also used a maximum value of extinction (A_V) which was determined by tracing back the current location of the YSOs on $J/(J-H)$ diagram to the intrinsic locus of dwarf along the reddening vector (Samal et al. 2010). The minimum value of foreground extinction in the direction of Stock 8 is taken as 1.2 mag.

We have fitted SEDs for 11 identified YSOs. The WISE data for stars with IDs V19, V26, V37, V45, V84, V85, V90, V91, V110, V113, and V128 were not available. The SEDs of two sources V96 and V99 are shown in Fig. 8 as an example. As expected, the SED models show a high degree of degeneracy in the absence of mid/far infrared and millimeter data, however, the SEDs of 4 identified CTTSs (V106, V99, V125 and V61) and 2 probable HAeBe sources indicate the presence of NIR/MIR-excess emission, possibly due to circumstellar disk. It is not possible to characterize all the SED parameters from the model due to limited data points. However, the SED models fit the observed data fairly well in the wavelength range from 0.4 μm to 12 μm , and we expect that the age and mass estimations of the YSOs should be constrained well enough. Table 4 lists the age and mass estimated from the SED analysis. These parameters have been obtained using the criterion $\chi^2 - \chi_{min}^2 \leq 2N_{data}$ weighted by $e^{(-\chi^2/2)}$ of each model as done in Samal et al. (2012), where χ_{min}^2 is the goodness-of-fit parameter for the best-fit model and N_{data} is the number of input observational data points. Table 4 indicates that age and mass estimations using the SED models are higher by ~ 2 times in comparison to the es-

Table 5. The effective temperature (T_{eff}), bolometric correction (BC), bolometric magnitude (M_{bol}), luminosity (L).

ID	$\log T_{\text{eff}}$	BC (mag)	M_{bol} (mag)	$\log(L/L_{\odot})$
V23	3.996	-0.07031	0.02169	1.884
V38	4.060	-0.4844	-0.6554	2.155
V42	4.165	-1.125	-1.26	2.397
V55	4.025	-0.2422	0.8918	1.536
V56	4.235	-1.508	-2.42	2.861
V59	4.123	-0.8281	0.4519	1.712
V64	4.054	-0.3359	0.9061	1.53
V66	3.963	0.01562	1.394	1.335
V68	4.073	-0.6094	-1.18	2.365
V76	3.95	0.1406	0.1466	1.834
V79	4.029	-0.2266	0.6904	1.617
V80	3.987	-0.0625	0.3485	1.753
V81	3.997	-0.04688	1.55	1.273
V93	3.977	-0.01562	-0.4896	2.089
V94	4.234	-1.438	-2.048	2.712
V103	4.056	-0.5156	-0.1916	1.969
V105	4.093	-0.5938	0.03275	1.906
V107	4.057	-0.3984	0.09256	1.856
V109	4.294	-1.727	-2.1	2.733
V114	4.071	-0.5	0.329	1.761
V116	4.104	-0.7578	-0.2288	1.984
V120	4.068	-0.5391	-0.1251	1.943
V121	4.076	-0.5391	0.9369	1.518
V130	4.411	-2.25	-6.097	4.332

timates based on the $V/(V-I)$ CMD. Since photometry in optical bands in comparison to NIR bands has better accuracy and variables studied in the present study have relatively lower extinction, the age and mass estimated from $V/(V-I)$ CMD seem to be reliable. Table 4 also indicates that the mass and age estimates using $V/(V-I)$ CMD have lesser uncertainties in comparison to those obtained from the SED fitting.

6. NATURE OF VARIABLE STARS

Figs. 9, 10, 11 and 12 display phased light curves of variable stars identified as the MS stars, PMS population of cluster, field population and unclassified, and probable BP population of Norma-Cygnus arm, respectively, where the average magnitude in 0.01 phase bin is represented by filled circles and error bars represent standard deviation of mean magnitude in particular bin.

6.1. MS Variables

In order to characterize the MS variables associated with the cluster region, we have plotted them in H-R diagram (Fig. 13). Fig. 13 shows the $\log(L/L_{\odot}) / \log T_{\text{eff}}$ diagram (H-R diagram) for the MS variables. In Fig. 13, we could not plot 4 MS variables V29, V92, V102 and V129 due to unavailability of their $U - B$ colours. The luminosity and temperature of a star is determined as follows. First of all, we have determined the intrinsic ($B - V$) colours with the help of the Q -

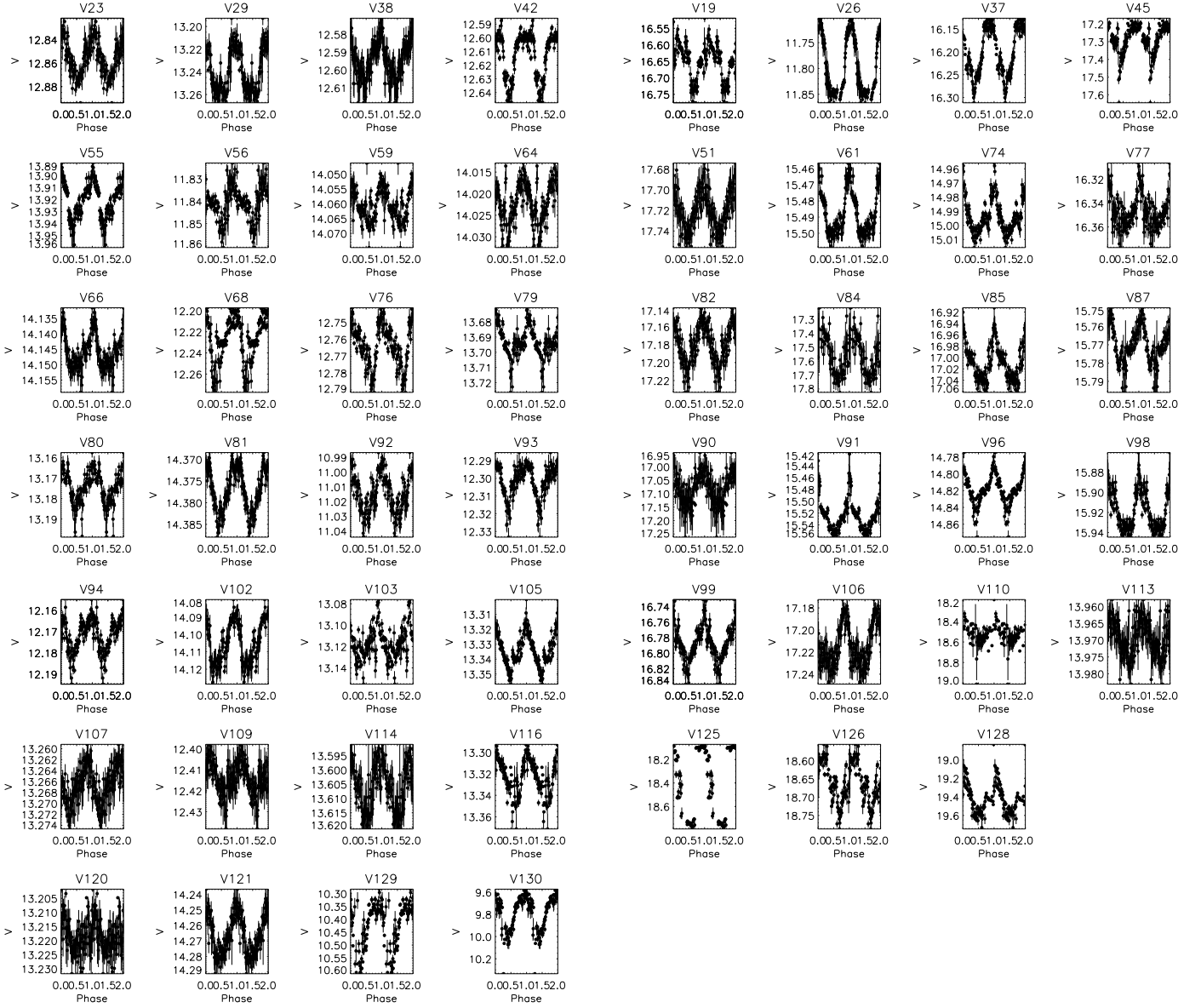


Figure 9. The V band phased light curves of MS variable stars.

method (Gutierrez-Moreno 1975). The absolute magnitude, M_V was obtained assuming distance modulus of the Stock 8 as 12.8 mag. To convert M_V into luminosity ($\log L/L_\odot$) it is necessary to know the bolometric correction (BC). The BC is determined from the effective temperature as it is a function of temperature. The effective temperature T_{eff} was determined using the relation between T_{eff} and intrinsic ($B - V$)

Figure 10. The V band phased light curves of PMS variable stars.

colour by Torres (2010). The BC has been calculated using T_{eff} with the help of Torres (2010) relation. After that luminosity of the stars was determined from a relation $\log(L/L_\odot) = 0.4(M_{\text{bol}} - M_{\text{bol}\odot})$, where $M_{\text{bol}} = M_V + BC$, and M_{bol} and $M_{\text{bol}\odot}$ are bolometric magnitudes for the star and Sun, respectively. In the case of Sun, the bolometric magnitude $M_{\text{bol}\odot}$ was considered as 4.73 mag (Torres 2010). Thus, the deter-

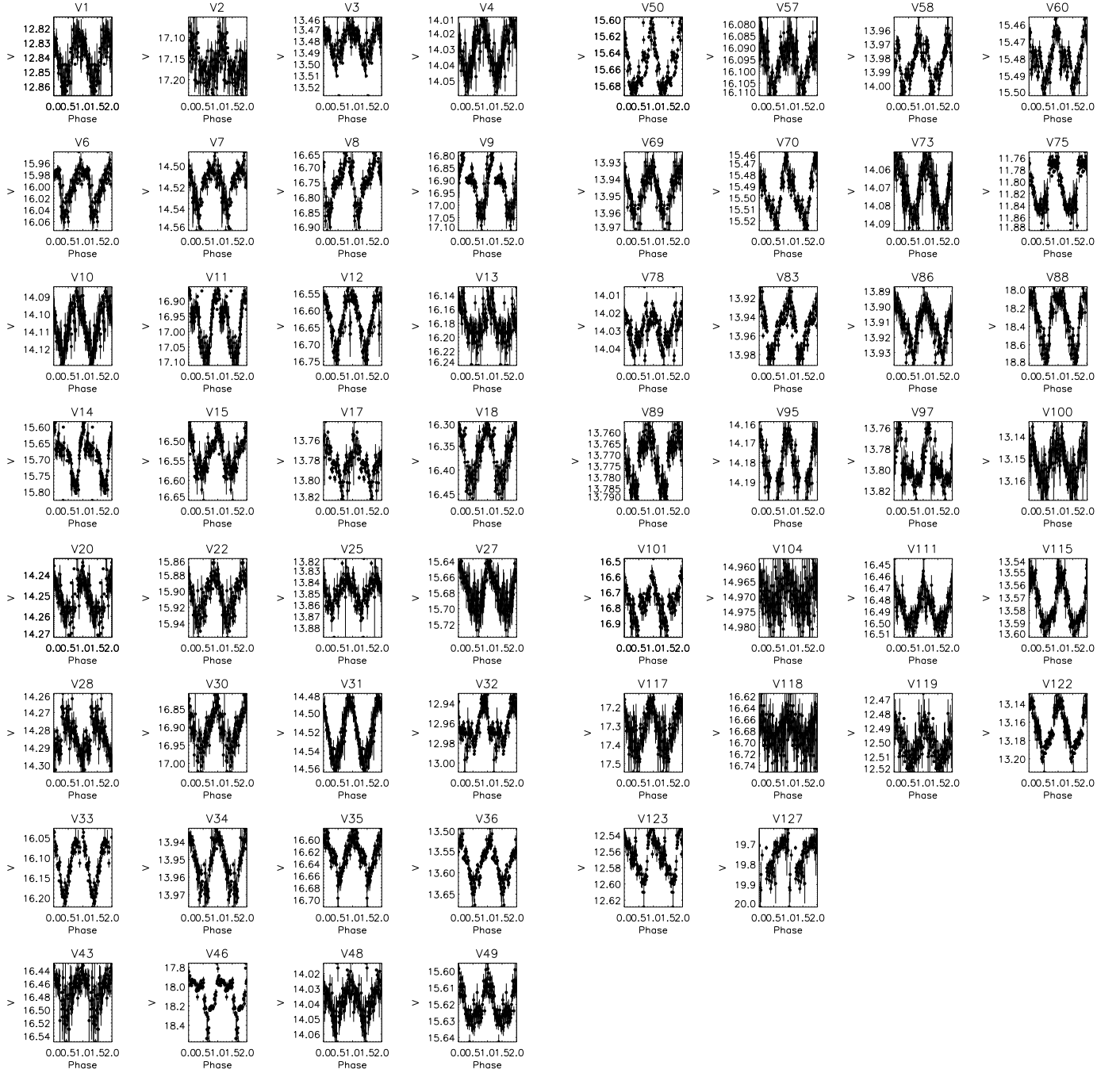


Figure 11. The V band phased light curves of unclassified and field variables.

Figure 11. continued.

mined parameters such as T_{eff} , BC , M_{bol} and $\log L/L_{\odot}$ for MS stars are given in Table 5.

Fig. 13 also shows the theoretical slowly pulsating B (SPB) instability strip (continuous curve), location of β Cep stars (dashed curve) and empirical δ Scuti instability strip (dotted curve) taken from Balona et al. (2011; references therein). Twenty eight variables are found to be MS type stars associated with the cluster. The pe-

riods of these stars estimated in the present work range between 0.053 d to 0.450 d and amplitudes range from 0.01 to 0.38 mag.

In the H-R diagram (cf. Fig. 13), the location of MS variable stars indicates that 7 stars (V38, V42, V56, V68, V94, V109 and V116) could be SPB stars, whereas star V130 could be a β Cep variable. Two stars V66 and V76 are found to lie in the δ Scuti region and these could

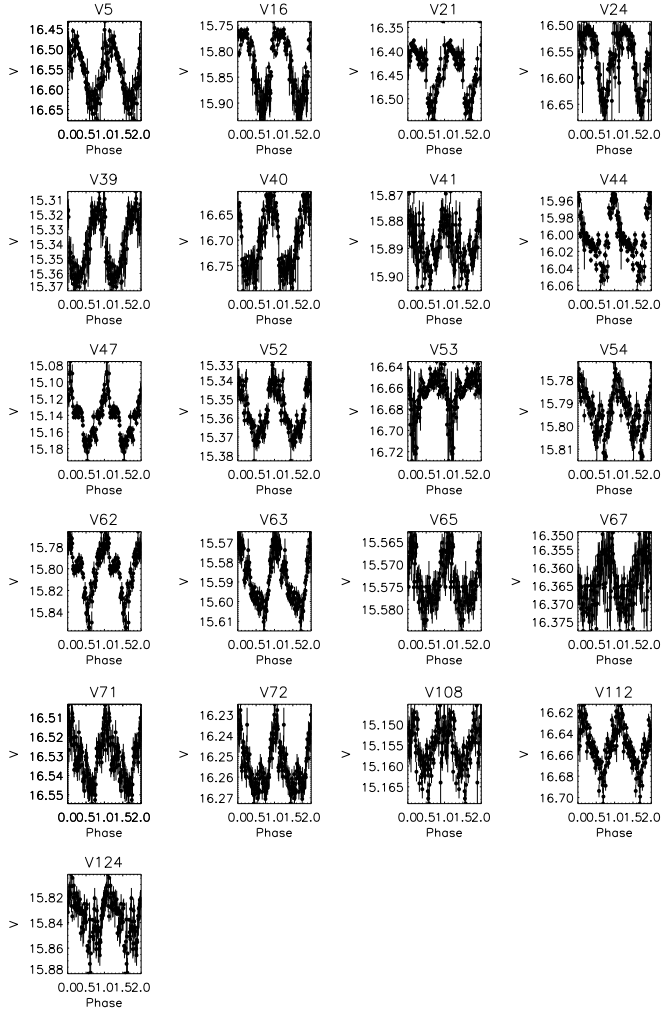


Figure 12. The V band phased light curves of variable stars associated to the BP population.

be δ Scuti variables. Fourteen stars V23, V55, V59, V64, V79, V80, V81, V93, V103, V105, V107, V114, V120, and V121 are located in the gap present between SPB and δ Scuti instability region. In the case of the open cluster NGC 3766, Mowlavi et al. (2013) have found a large population of new variable stars between SPB stars and the δ Scuti stars, the region where no pulsations were expected on the basis of theoretical models.

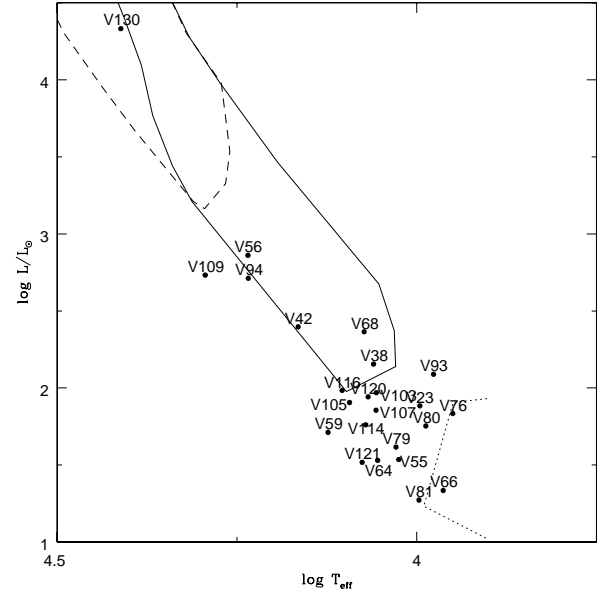


Figure 13. $\log(L/L_{\odot})/\log T_{\text{eff}}$ diagram of the cluster Stock 8 for the probable MS variable stars. The continuous and dotted curve are the instability strip for SPB and δ Scuti stars, respectively and dashed curve shows the location of β Cep stars (for references see Balona et al. 2011).

The findings of Mowlavi et al. (2013) were further supported by Lata et al. (2014) in the case of young cluster NGC 1893. Mowlavi et al. (2013) have reported periods of these variable stars in the range of 0.1 to 0.7 d, with amplitudes between 1.0 to 4.0 mmag, whereas Lata et al. (2014) found the periods of a new class of variables ranging from 0.17 to 0.58 d with an amplitude of variation in the range 0.007 to 0.019 mag. Periods and amplitudes of these new class variables identified in the present work have range of 0.064 to 0.364 d and ~ 0.01 to ~ 0.04 mag, respectively.

The origin of variability of these stars could be pulsation. One of the probable causes of pulsation in these stars could be rapid rotation which alters the internal conditions of a star enough to sustain stellar pulsations. Another cause for the brightness variation in these stars might be the presence of spots on the surface of such rotating stars and that these spots would induce light variations as the star rotates. But hot stars are not expected to be active, and no theory can currently explain how spots could be produced on the surface of such stars. Balona et al. (2011) analyzed light curves of 48 B-type stars observed by Kepler and did not find any star lying between the red end of the SPB stars and the blue end of δ Scuti type stars.

6.2. PMS variables

In the present work, we classify 23 stars as probable PMS stars (cf. Table 3). The identified PMS variables have ages and masses in the range of 0.2 - 5.8 Myr and 0.5 - 2.75 M_{\odot} respectively, which are comparable to those of TTSSs. The majority of these stars are located in ‘F’ region of $(J - H)/(H - K)$ TCD. As discussed in Section 3, the ‘F’ region may contain some Class II sources which have small NIR excess. In fact, figure 3a by Pandey et al. (2014) in the case of the young open cluster NGC 1893 reveals that the ‘F’ region contains a significant amount of Class II sources. A careful view of figure 3b by Pandey et al. (2014) manifests that almost all the Class III YSOs are located toward the left side of the ‘F’ region, whereas a significant number of Class II YSOs can be noticed towards the right side of the ‘F’ region. Hence, we subdivided ‘F’ region, shown with a dot-short dash line in Fig. 5, into ‘F1’ and ‘F2’ regions. The PMS stars lying in the ‘F2’ region are also considered as Class II sources.

The star V125 lies in the ‘T’ region in $(J - H)/(H - K)$ TCD (Fig. 5) hence should be a CTTS, likewise stars V61, V99, V106 and V110 that lie in the ‘F2’ region. The amplitudes of stars V61, V99, V106 and V110 are in the range from 0.026 - 0.412 mag, whereas amplitude of star V125 is found as 0.360 mag. The periods of these CTTSs are in the range of 0.128 - 0.648 d. The location of stars V96 and V98 suggests that these could be HAeBe stars. The masses and ages of these sources are 2.13 M_{\odot} , 2.75 M_{\odot} and 3.13 Myr, 1.92 Myr, respectively. The period and amplitude of V96 and V98 are estimated as 0.159 d, 0.121 d and 0.051 mag, 0.042 mag, respectively. In the case of NGC 1893, Lata et al. (2012) have identified 2 probable HAeBe stars with periods 0.30 d and 0.47 d and amplitudes 0.01 mag and 0.02 mag. Stars numbered V19, V26, V37, V45, V51, V74, V77, V82, V84, V85, V87, V90, V91, V113, V126, and V128 lie in the ‘F1’ region and could be WTTSs. These WTTSs have amplitude in the range of 0.013 - 0.456 mag and periods lie in the range of 0.095 - 0.498 d.

The present sample of TTSSs manifests that CTTSs have amplitude in the range of 0.039 - 0.288 mag, whereas the amplitude of majority of WTTSs varies from 0.013 to 0.242 mag. This indicates that the brightness of CTTSs varies with larger amplitude in comparison to WTTSs. This result is in agreement with the previous studies (Grankin et al. 2007, 2008; Lata et al. 2011, 2012 and 2016). As discussed, e.g., by Carpenter, Hillenbrand & Skrutskie (2001) the larger amplitude in the case of CTTSs could be due to the presence of hot spots on the stellar surface produced by an accretion mechanism. Hot spots cover a small fraction of the

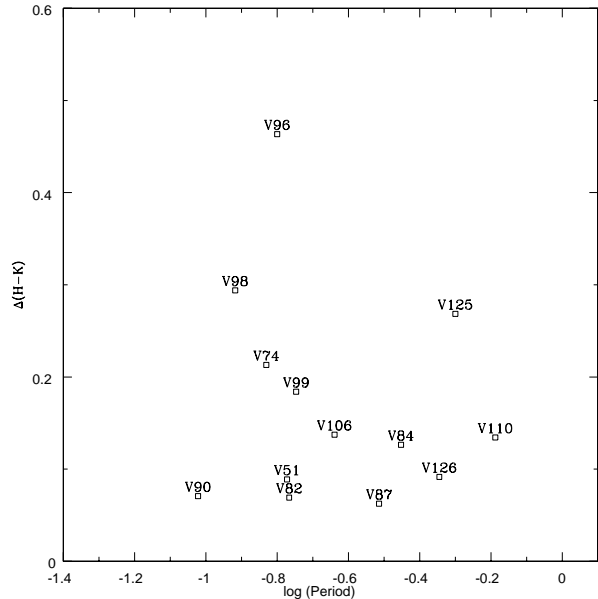


Figure 14. $\Delta(H - K)$ vs rotation period.

stellar surface but with a higher temperature causing larger amplitude of brightness variations. The smaller amplitude in WTTSs suggests dissipation of their circumstellar discs or these stars might have cool spots on their surface which are produced due to convection and differential rotation of star and magnetic field. The results obtained in the present study are in agreement with work reported by Grankin et al. (2007, 2008). These results also match with that of Lata et al. (2011, 2012 and 2016).

6.3. Field, Blue Plume Population in Norma-Cygnus arm and non classified stars

In the present sample, 58 variables are found to be field and unclassified population lying towards the direction of Stock 8. These variables have periods ranging from 0.051 d to 0.549 d. The period and amplitude of star V31 which belongs to unclassified stars are 0.113 d and 0.042 mag, respectively. The light curve of V31 is found to be similar to that of δ Scuti type variables. The probable BP variables namely stars V5, V16, V21, V24, V39, V40, V41, V44, V47, V52, V53, V54, V62, V63, V65, V67, V71, V72, V108, V112, and V124 have period and amplitude in the range of 0.093 d to 0.378 d and 0.011 to 0.123 mag, respectively. The characteristics of these stars as well as their light curves indicate that they could be β Cep or SPB stars.

7. ROTATION AND $\Delta(H - K)$

In the case of PMS stars, it is suggested that the magnetic star-disk interaction could drive the angular momentum of the star (Königl 1991). The loss of angular

momentum due to accretion-related processes suggests that accreting stars should be slower rotators than non-accreting ones. A few studies have hinted to a correlation between the rotation rate and the NIR/IR excess of PMS objects (Edwards et al. 1993, Lamm et al. 2005, Rebull et al. 2006, 2014, Lata et al. 2016). However, Stassun et al. (1999) in the case of Orion Nebula Cluster (ONC) and Cieza & Baliber (2006) in the case of IC 348 did not find any correlation between accretion and rotation.

The conflicting results, whether a correlation exists between rotation and accretion process in PMS or not, may be due to several causes e.g. mass of PMS stars; statistical robustness of the data etc. could be some of the reasons. Cieza & Baliber (2007) have shown that if effect of mass is removed, a clear trend in the disk fraction with period can be observed in NGC 2264 and Orion nebula clusters. Venuti et al. (2015, 2016) have found that the connection between rotational properties and accretion traced via UV excess measurements is consistent with earlier findings (based on IR excess measurements) in the sense that fast rotators are typically devoid of dusty disks.

The data in the present work are very small, however, a plot between NIR excess index, $\Delta(H - K)$ and period in Fig. 14 indicates no correlation between $\Delta(H - K)$ and period for short period variables. Where $\Delta(H - K)$ is the horizontal displacement of the YSO location from the left reddening vector of ‘F’ region in the $(J - H)/(H - K)$ TCD (Fig. 5). It is worthwhile to mention here that the plot between UV excess and rotation period by Venuti et al. (2016, see figure 11) does not show any correlation between UV excess and period for PMS stars having period $\lesssim 1$ day, which is consistent with the present results.

8. SUMMARY

In the current study, we have presented time series photometry of 130 variables in the field of young open cluster Stock 8. We identified 51, 50 and 29 stars as members of the cluster, non members and unclassified, respectively. Member stars are categorized as 28 MS and 23 PMS stars. Twenty one of 50 variables identified as field star population could belong to BP population. Of 28 MS variables, 1, 2, 7 and 14 stars are classified as β Cep, δ Scuti, SPB, and new class variables, respectively. Since the variability behaviour for 14 new class variables is not easily explained, additional photometric monitoring of these objects is desirable. Four MS variables remain uncharacterized in the present work. Five and 2 of 23 PMS variables are found to be CTTSs and HAeBe stars, respectively, whereas 16 PMS stars

are found to be WTTSs. For the majority of these PMS variables, the ages are found to be $\lesssim 5$ Myr while masses are in the range from 0.50 to 2.8 M_{\odot} . Based on its light curve shape, period and amplitude, star V31 could be classified as a δ Scuti variable. No correlation between $\Delta(H - K)$ and rotation period is found for short period PMS variables.

9. ACKNOWLEDGMENT

Authors are thankful to the anonymous referee for useful scientific suggestions/comments. This work has made use of data obtained at the Thai National Observatory on Doi Inthanon operated by NARIT. AKP is thankful to the NARIT for providing support during his visit to NARIT.

REFERENCES

- Balona L. A., Pigulski A., Cat P. De, Handler G., Guti rrez-Soto J., Engelbrecht C. A., Frescura F., Briquet M., et al., 2011, MNRAS, 413, 2403
 Bessell M. S., Brett J. M., 1988, PASP, 100, 1134
 Bouvier J. et al., 1997, A&A, 318, 495
 Carpenter J. M., Hillenbrand L. A., Skrutskie M. F., 2001, AJ, 121, 3160
 Chauhan N., Pandey A. K., Ogura K., Ojha D. K., Bhatt B. C., Ghosh S. K., Rawat P. S., 2009, MNRAS, 396, 964
 Cieza L., Baliber N., 2006, ApJ, 649, 862
 Cieza L., Baliber N., 2007, ApJ, 671, 605
 Cohen J. G., Persson S. E., Elias J. H., Frogel J. A., 1981, ApJ, 249, 481
 Cutri R. M., et al. VizieR Online Data Catalog: WISE All-Sky Data Release, VizieR On-line Data Catalog: II/311. Vol. 2311. 2012. p. 0.
 Cutri R. M., Skrutskie M. F., van Dyk S., Beichman C. A., Carpenter J. M., Chester T., Cambresy L., Evans T., Fowler J., Gizis J., et al., 2003, 2MASS All Sky Catalog of point sources
 Dhillon V. S., Marsh T. R., Atkinson D. C., Bezawada N., Bours M. C. P., Copperwheat C. M., Gamble T., Hardy L. K., Hickman R. D. H., Irawati P., Ives D. J., Kerry P., Leckngam A., Littlefair S. P., McLay S. A., O’Brien K., Peacocke P. T., Poshyachinda S., Richichi A., Soonthornthum B., Vick A., 2014, MNRAS, 444, 4009
 Duquenois A. and Mayor M., 1991, A&A, 248, 485
 Edwards S., Strom S. E., Hartigan P., Strom K. M., Hillenbrand L. A., Herbst W., Attridge J., Merrill K. M., Probst R., Gatley I., 1993, AJ, 106, 372
 Girardi L., Bertelli G., Bressan A., Chiosi C., Groenewegen M. A. T., Marigo P., Salasnich B., & Weiss A., 2002, A&A, 391, 195

- Grankin K. N., Melnikov S. Yu., Bouvier J., Herbst W., Shevchenko V. S., 2007, *A&A*, 461, 183
- Grankin K. N., Bouvier J., Herbst W., Melnikov S. Y., 2008, *A&A*, 479, 827
- Gutiérrez-Moreno A., *PASP*, 1975, 87 805
- Herbst W., Herbst D. K., Grossman E. J., Weinstein D., 1994, *AJ*, 108, 1906
- Jose J., Pandey A. K., Ojha D. K., Ogura K., Chen W. P., Bhatt B. C., Ghosh S. K., Mito H., Maheswar G., Sharma S., 2008, *MNRAS*, 384, 1675
- Jose J. Herczeg G. J., Samal M. R., Fang Q., Panwar, N., 2017, *ApJ*, 836, 98
- Joy A. H., 1945, *ApJ*, 102, 168
- Königl A., 1991, *ApJ*, 370, 39
- Lamm M. H., Mundt R., Bailer-Jones C. A. L., Herbst W., 2005, *A&A*, 430, 1005
- Lata S., Pandey A. K., Maheswar G., Mondal S., Kumar B., 2011, *MNRAS*, 418, 1346
- Lata S., Pandey A. K., Chen W. P., Maheswar G., Chauhan N., 2012, *MNRAS*, 427, 1449
- Lata S., Yadav Ram Kesh, Pandey A. K., Richichi A., Eswaraiyah C., Kumar B., Kappelmann N., Sharma S., 2014, *MNRAS*, 442, 273
- Lata S., Pandey A. K., Panwar Neelam, Chen W. P., Samal M. R., Pandey J. C., 2016, *MNRAS*, 456, 2505
- Lomb N. R., 1976, *ApSS*, 39, 447
- Menard F., Bertout C, 1999, in Lada C. J., Kylafis N. D., eds, *The Origin of Stars and Planetary Systems*. Kluwer Academic Publishers, Dordrecht, p. 341
- Meyer M. R., Calvet N., Hillenbrand L. A., 1997, *AJ*, 114, 288
- Mowlavi N., Barblan F., Saesen S., Eyer L., 2013, *A&A*, 554, 108
- Pandey A. K., Sharma S., Ogura K., 2006, *MNRAS*, 373, 255
- Pandey A. K., Samal M. R., Yadav R. K., Richichi A., Lata S., Pandey J. C., Ojha, D. K., Chen W. P., 2014, *NewA*, 29, 18
- Percy J. R., Esteves S., Glasheen J., Lin A., Long J., Mashintsova M., Terziev E., Wu S., 2010, *J. Am. Assoc. Var. Star Observers*, 38, 151
- Richichi A., Irawati P., Soonthornthum B., Dhillon V. S., Marsh T. R., 2014, *AJ*, 148, 100
- Rebull L. M., Stauffer J., Megeath S., Hora J. L., Hartmann L., 2006, *ApJ*, 646, 297
- Rebull L. M., Cody A. M., Covey K. R., et al., 2014, *AJ*, 148, 92
- Robitaille T. P., Whitney B. A., Indebetouw R., Wood K., 2007, *ApJS*, 169, 328
- Robitaille T. P., Whitney B. A., Indebetouw R., Wood K., Denzmore P., 2006, *ApJS*, 167, 256
- Samal M. R., Pandey A. K., Ojha D. K., et al., 2010, *ApJ*, 714, 1015
- Scargle J. D., 1982, *ApJ*, 263, 835
- Sesar B. et al, 2007, *AJ*, 134, 2236
- Siess L., Dufour E., Forestini M., 2000, *A&A*, 358, 593
- Stetson P. B., 1987, *PASP*, 99, 191 Stetson P. B, 1992, *J. R. Astron. Soc. Can.*, 86, 71
- Stassun Keivan G., Mathieu R. D., Mazeh T., Vrba F. J., 1999, *AJ*, 117, 2941
- Torres G., *AJ*, 2010, 140, 1158
- Venuti L., Bouvier J., Irwin J., Stauffer J. R., Hillenbrand L. A., Rebull L. M., Cody A. M., Alencar S. H. P., Micela G., Flaccomio E., Peres G., 2015, *A&A*, 581, 66
- Venuti L., Bouvier J., Cody A. M., Stauffer J. R., Micela G., Rebull L. M., Alencar S. H. P., Sousa A. P., Hillenbrand L. A., Flaccomio E., 2016, *arXiv161008811V*
- Waelkens C., 1991, *A&A*, 246, 453